IEEE Photonics Journal
An IEEE Photonics Society Publication

Open Access

Bidirectional Bend Sensor Employing a Microfiber-Assisted U-Shaped Fabry-Perot Cavity

Volume 9, Number 3, June 2017

Zhiyong Bai
Shecheng Gao
Mi Deng
Zhe Zhang
Mingquan Li
Feng Zhang
Changrui Liao
Ying Wang
Yiping Wang

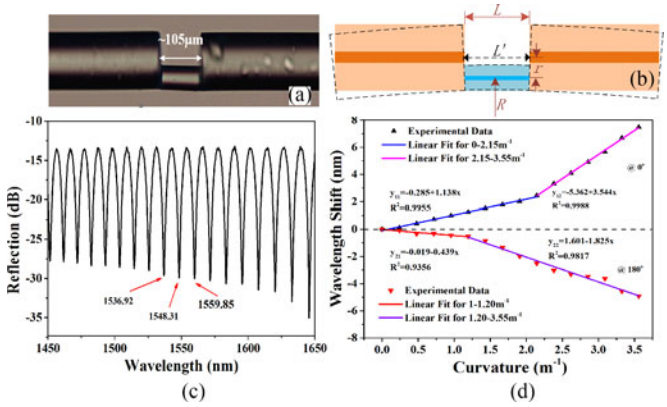

DOI: 10.1109/JPHOT.2017.2690668
1943-0655 © 2017 IEEE

Bidirectional Bend Sensor Employing a Microfiber-Assisted U-Shaped Fabry-Perot Cavity

Zhiyong Bai,[1] Shecheng Gao,[2] Mi Deng,[1] Zhe Zhang,[1] Mingquan Li,[1] Feng Zhang,[1] Changrui Liao,[1] Ying Wang,[1] and Yiping Wang[1]

[1]Key Laboratory of Optoelectronic Devices and Systems of Ministry of Education and Guangdong Province, College of Optoelectronic Engineering, Shenzhen University, Shenzhen 518060, China
[2]Department of Electronic Engineering, Jinan University, Guangzhou 510632, China

DOI:10.1109/JPHOT.2017.2690668

Manuscript received February 13, 2017; revised March 26, 2017; accepted March 31, 2017. Date of publication April 13, 2017; date of current version May 9, 2017. This work was supported in part by the National Natural Science Foundation of China under Grant 61425007, Grant 61377090, Grant 61575128, Grant 61605129, and Grant 61605123; in part by the Guangdong Science and Technology Department under Grant 2014A030308007, Grant 2014B050504010, Grant 2015B010105007, and Grant 2015A030313541; in part by the China Postdoctoral Science Foundation under Grant 2015M582404 and Grant 2015M582406; in part by the Science and Technology Innovation Commission of Shenzhen under Grant ZDSYS20140430164957664, Grant GJHZ20150313093755757, Grant KQCX20140512172532195, and Grant JCYJ20150324141711576; and in part by the Pearl River Scholar Fellowships. (Corresponding author: Yiping Wang (ypwang@szu.edu.cn).

Abstract: A bidirectional bend sensor based on U-shaped Fabry-Perot interferometer (UFPI) is experimentally demonstrated. The UFPI is constructed by eccentrically splicing a section of microfiber between two cleaved standard single mode fiber end faces serving as mirrors. A preliminary theoretic analysis of bending response of UFPI is presented. The bend and temperature sensing properties are measured. The theoretical and experimental investigation demonstrates the bending direction discrimination and the monotonous sensing characteristic in a single direction along or opposite to the cavity opening direction. The proposed bend sensor with more compact ($\sim$105 μm in length) and easier fabrication presents a high contrast of the interferometer fringes and low temperature sensitivity of 1.21×10^{-3} nm/°C.

Index Terms: Bend sensor, Fabry-Perot interferometry (FPI), optical fiber sensors.

1. Introduction

A fiber-based Fabry-Perot interferometer (FPI) with mirrors separated by air is usually defined as extrinsic FPI (EFPI) [1], which has been intensively investigated for various applications in the physical [2], [3], chemical [4], [5], and biological [6], [7] sensing fields, due to their unique characteristics such as simple configurations, compactness, and endurance for high temperature and high pressure environments [8], [9]. Many types of EFPI have been proposed, such as bonding two cleaved fibers into a small-diameter tube [10], splicing a hollow-core fiber or hollow-core photonic crystal fiber between two standard single-mode fibers (SMFs) [11], [12], inducing a rectangular air cavity during splicing SMFs [9], forming a spherical air micro-cavity by splicing a photonic crystal fiber with an SMF or splicing two SMFs [13]–[15], and ablating a cavity in the SMF by femtosecond

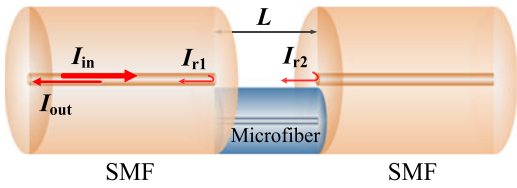

Fig. 1. Schematic of UFPI. The two end faces of the SMF serve as mirrors, and the microfiber is the connecting arm.

laser [16]. These EFPIs are usually employed as strain, refractive index, and high temperature sensors.

The measurement of curvature is likewise attracting intense interest in the fiber sensing field, because that the bending deformation is of great significance in the area of aerospace, machinery, and building structural health monitoring [17], [18]. Several fiber-based bend sensing methods have been proposed and achieved by mainly using fiber Bragg grating [19], [20], long-period grating [21], [22], and fiber-mode interferometer [23], [24]. However, the study on bending measurement employing EFPI is not sufficient, and it is difficult to look up the reports on this topic, which may result from the comprehensive action of a difficulty to bent the minisize EFPI, low bending sensitivity, poor mechanical strength, and so on.

In this paper, we present a bidirectional bending sensor employing the EFPI fabricated by splicing a section of microfiber with two SMF. The opening air cavity between two SMF end faces serves as the FP cavity and a direct sensing head. The microfiber is prepared by tapering SMF to around 54 μm in diameter to avoid touching the SMF core during the eccentrically splicing. The proposed FP cavity possesses an asymmetric structure and displays a U-like shape, and thus named as U-shape FPI (UFPI) in this paper. An approximately theoretic analysis is obtained. The theoretic result suggests a capability of detecting the bending amplitude and determining the sense along or opposite to the cavity opening direction. The bending and temperature sensing characteristics of UPI are measured. When the UFPI is bent, the interference fringes dips display a blue or red shift according to the bend vector along or opposite to the opening direction of the cavity, and the wavelength shift monotonously changes with respect to curvature in a single direction. The temperature sensitivity is only 0.00121nm/°C, which indicates a higher precision of bending measurement than that of other bend sensors based on Fiber grating [19]–[22] and interferometry [23], [24].

2. The Design of UFPI and Its Sensing Principle

Fig. 1 depicts the schematic of the proposed UFPI which is composed of two cleaved SMF end faces as mirrors and a section of microfiber as a connector. The microfiber is spliced with the two end faces by the arc discharge fusion to enhance the mechanical strength of UFPI. In order to make sure that the light propagation comply with the principle of FPI, the microfiber is eccentrically spliced to the SMF end faces to avoid touching the SMF cores.

When propagating through the UFPI, the incident light I_{in} is respectively reflected by two mirrors and the reflected light interferes with each other in the SMF core resulting in an interference pattern at the output. Because of the low reflectivity of air and silica interface, the rigorous multiple beams interference of FPI is approximately simplified as double beams interaction, and thus the total output intensity I_{out} of the reflected light after passing through the UFPI can be written as

$$I_{out} = I_{r1} + I_{r2} + 2\sqrt{I_{r1} I_{r2}} \cos(4\pi n_{air} L / \lambda) \tag{1}$$

where I_{r1},I_{r2} is the first reflected intensity at the two reflectors, respectively; L is the length of microfiber and the U-shape cavity; n_{air} is the refractive index of air; and λ is the free space wavelength of the input laser beam. When $4\pi n_{air} L / \lambda = (2m + 1)\pi$, $m = 1, 2, \ldots$, the interference dips appear

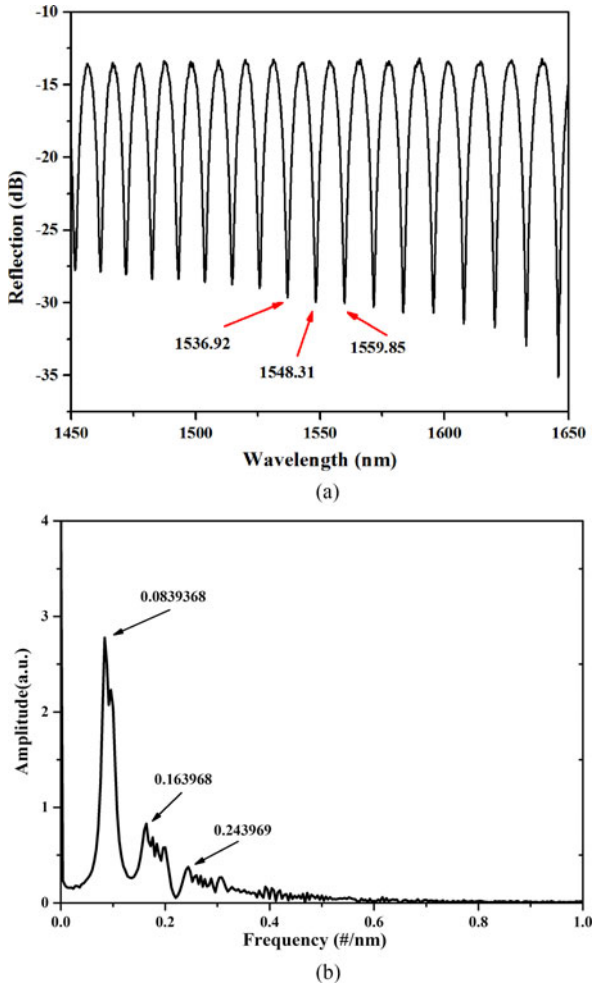

Fig. 2. (a) Interference spectrum of UFPI with an assistant microfiber of 105 μm in length and 54 μm in diameter and (b) its space frequency spectrum.

at the wavelengths λ_m satisfied by

$$\lambda_m = \frac{4\pi n_{\text{air}} L}{(2m+1)\pi} \tag{2}$$

and the wavelength difference between adjacent dips [defined as free spectral range (FSR)] is expressed by

$$FSR = \frac{\lambda_m \lambda_{m-1}}{2\pi n_{\text{air}} L}. \tag{3}$$

In the interference pattern of UFPI depicted in Fig. 2(a), the position and separation of a series of dips are determined by (2) and (3), respectively. A fast Fourier transform is operated on this reflected spectrum to offer a deep sight into the frequency components as shown in Fig. 2(b). From the proportion of amplitude possessed by every frequency component, it can be described as the power of the reflected light is mainly concentrated in lowest frequency component, and the proportion of that in high-frequency ones quickly fade away with the increase of frequency. Obviously, the power in the lowest frequency component mainly results from the first reflection of UFPI, and the light power of high-frequency ones is induced from multiple reflection and can be

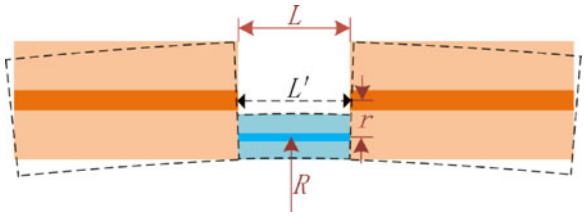

Fig. 3. Schematic diagram of UFPI under bending in 0° direction. L is the original cavity length, R is the bend radius of microfiber, r is the eccentrically distance between two cores of the microfiber and SMF, and L' is variational cavity length under bending.

neglected in an un-strict theoretic description as the preceding assumption on the double beam interference.

When the UFPI is subjected to external perturbations, the refractive index n_{air} inside the cavity or the cavity length L will variate, as a result, the dips position and the intensity of the interference spectrum correspondingly change. Therefore, the environment parameters can be monitored by tracking the variations of the reflected spectrum. When a bend is applied to the UFPI, the refractive index of air in the cavity keeps a constant, but the cavity length will be changed because of the geometric deformation. From the (2), the wavelength shift $\Delta\lambda_m$ of the reflected spectrum rooted in the variation of cavity length ΔL can be derived as

$$\Delta\lambda_m = \lambda_m \Delta L / L . \tag{4}$$

Since ΔL is directly related to the bending radius R via a geometric transformation, an intuitionistic relationship between $\Delta\lambda_m$ and R can be expected.

A bending UFPI is schematically shown in Fig. 3. For a convenient description, the bend opposite to the cavity opening direction as illustrated by a dash line in Fig. 3 is denoted 0° direction, and the reverse direction, i.e., along cavity opening direction, is named as 180° direction. Other geometry parameters marked in Fig. 3 are also described as follows: L is the original cavity length, R is the bend radius of microfiber, r is the eccentrically distance between two cores of the microfiber and SMF, and L' is the variational cavity length under bending.

In this work, the microfiber length, i.e., the original cavity length L is assumed to be a constant. L' is approximately equal to the arc length between two end faces of SMF cores under small curvature. Thus, the actual bending radius of L' is $R + r$ in 0° direction and $R - r$ in 180° direction. In the state of bending free, $L' = L$. When the UFPI is bent, L' will be elongated or reduced according to the bending direction. Therefore, a relationship between L' and R can be built as $L'/(R \pm r) = L/R$ for a same sector angle. And then, $\Delta L = L' - L = \pm rCL$, where, $C = 1/R$ represents the bending curvature. Involving (4), $\Delta\lambda_m$ can be rewritten as

$$\Delta\lambda_m = \pm r\lambda_m C. \tag{5}$$

As can be seen from (5), a linear response of wavelength shift $\Delta\lambda_m$ to curvature C is presented, and it is noted that the red or blue shift of the wavelength is directly determined by the bending direction. When the UFPI is bent to 0° direction, the direct ratio relationship of $\Delta\lambda_m$ to C is valid, and thus the corresponding interference fringes shift towards longer wavelength. In contrast, the inverse ratio relationship is effective for 180° direction, and the corresponding interference fringes shift towards shorter wavelengths. Thus, the proposed UFPI-based bending sensor can tell the bending directions and evaluate the bending amplitude simultaneously.

3. Experiment Result and Discussion

The UFPI can be fabricated by the method presented in [4], which is summarily described as follows: First, a section of standard SMF (Corning SM-28e) is tapered to a microfiber with a desire waist diameter by the flame-brushing technique [25]. Second, the microfiber is cut off by a fiber cleaver

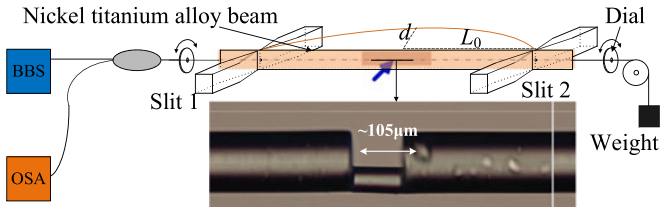

Fig. 4. Schematic diagram of the bending measurement setup. (Inset) Microscope image of UFPI.

and then eccentrically splicing to an SMF with a cleaved end face by an arc discharge fusion splicer with a manual splicing mode. Thirdly, a desired length of microfiber is achieved by a high-precision fiber cleaved setup [26] and splicing to another cleaved end face of SMF with the same method as the first joint.

A UFPI with L $=$ 105 μm and a microfiber diameter of 54 μm is fabricated, and its microscope image is illustrated in the inset of Fig. 4. The corresponding interference spectrum of the UFPI in the state of bending free is shown in Fig. 2(a), which has a contrast of more than 15 dB around 1550 nm, and the FSR $\approx$11.6 nm.

The bending measurement setup [27] for the UFPI is schematically shown in Fig. 4, which is mainly consisted of a high-elastic nickel-titanium alloy sheet to bend the fiber devices, a pair of slits to support the metal sheet and fiber, and two rotating disks to control bending directions. The SMF with a UFPI put in a capillary against the nickel-titanium alloy sheet is mounted on two aligned slits with a separation of $2L_0$, and passes through the two rotating disks. One of the SMF ends is fixed by the rotating disk A, and the other end goes through disk B and can freely move along the axial direction to eliminate the effect of strain. A metal rod fixed on a translating stage is made use of pushing the nickel-titanium alloy sheet to induce the UFPI bending along the direction shown as the arrow in Fig. 4. In this experiment, the length, external and inner radius of the capillary is 100 mm, 500 μm and 300 μm, respectively. The distance between the two slits is 90 mm. The bending curvature is calculated by considering the bent metal sheet as the arc of a circle. The chord length of the arc is $2L_0$, and the moving distance of the metal rod is d, thus the bending curvature C is expressed by $C = 2d/(d^2 + L_0^2)$. The UFPI is bent within a curvature range of 0–3.55 m^{-1} for two UFPI orientations. The evolutions of UFPI reflection spectra with respect to the bending curvatures are recorded by a Broadband Source (BBS) and an optical spectrum analyzer (OSA) and plotted in Fig. 5.

Fig. 5(a) shows the wavelength shift of reflection spectra, as the UFPI is bent to 0° direction. With the increase of C, the phase difference determined by the cavity length L' in (1) increases and then the interference shift towards longer wavelength.

Fig. 5(b) shows a blue shift of reflection spectra, as the UFPI is bent to 180° direction. With an increase of C, the cavity length, as well as the phase difference in (1), decrease, leading to the blue-shifted interference fringes. Therefore, it is safe to conclude that the UFPI can tell the bending directions by monitoring the wavelength shift of interference fringes. Moreover, during bending measurement, the contrast of UFPI displays a small fluctuation in the curvature rang of 0$-$3.55 m^{-1}, which indicates a convenience in practical application.

The bending sensitivity is also investigated by tracking one of the dips of the reflected interference fringe of UFPI under different bending curvatures and directions. The dip positioned at 1548.13 nm which is around 1550 nm as shown in Fig. 2(a) is monitored. In the curvature range of 0-3.55 m^{-1}, the dips totally shift from 1548.13 nm to 1555.02 nm for 0° direction, and from 1548.13 nm to 1543.94 nm for 180° direction. The wavelength shift of the reflected spectrum with respect to C is not always a linear relationship as the description of (5), and there is a step during the increase of curvature, which perhaps result from the dead zone existed in most bending sensor [20] and a deviation in the bending direction. To obtain the bending sensitivity of UFPI, the segmentation fitting is operated on the experimental data as shown in Fig. 6. For 0° direction, the bending sensitivities are

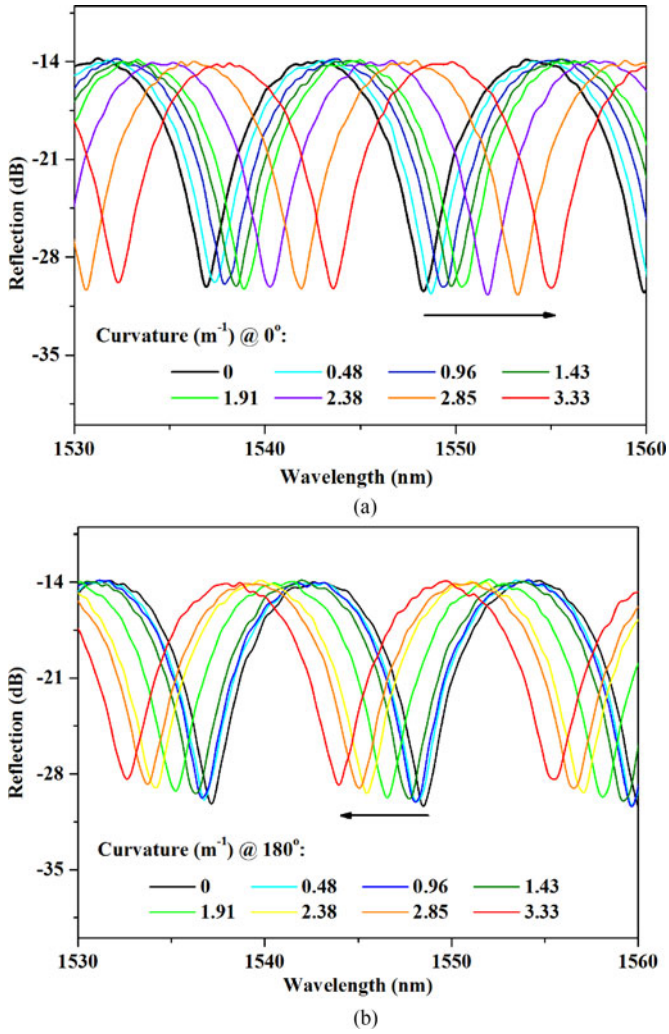

Fig. 5. Evolution of reflection spectra of the UFPI bent (a) to 0° and (b) to 180° direction.

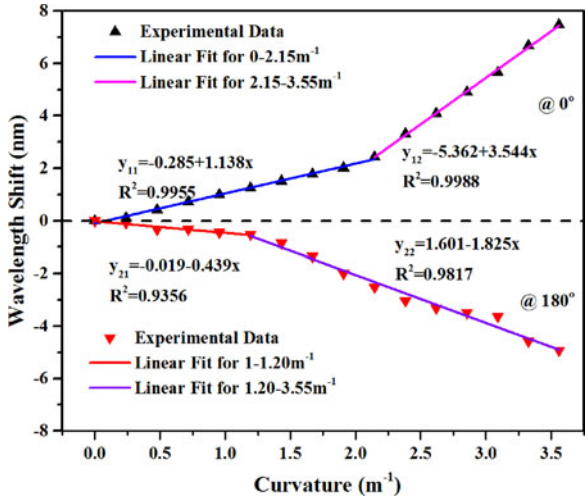

Fig. 6. Response of wavelength shift to curvature in 0° and 180° directions.

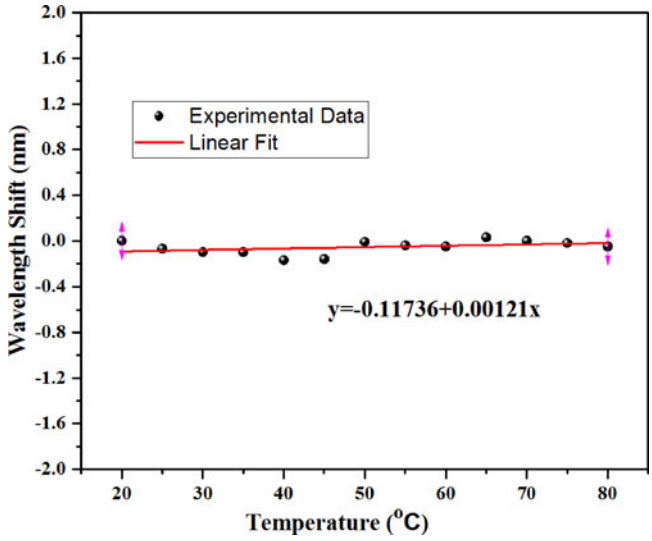

Fig. 7. Response of wavelength shift to temperature for a new UFPI sample with an assistant microfiber of 173 μm in length and 55 μm in diameter.

1.138 nm/m^{-1} and 3.544 nm/m^{-1} in the ranges of 0−2.15 m^{-1} and 2.15-3.55 m^{-1}, respectively. For the 180° direction, the bending sensitivities are −0.439 nm/m^{-1} and −1.825 nm/m^{-1} in the ranges of 0−1.20 m^{-1} and 1.20−3.55 m^{-1}, respectively. Although the ununiform sensitivity may induce some obstructions, the proposed bending sensor possesses a potential value in practical application for the characteristics of direction discrimination and monotonous response of wavelength shift to curvature.

The temperature behavior of this type of UFPI is also investigated. A new UFPI with the assisted microfiber dimension of 173 μm in length and 55 μm in diameter is heated in an electric furnace from 20 °C to 80 °C in air with an interval of 5 °C. The wavelength shift data were plotted with respect to temperature in Fig. 7, and subjected to linear fitting. The temperature sensitivity of the UFPI is around 1.21 $\times$ 10^{-3} nm/°C, which is a fairly low response.

4. Conclusion

We have proposed and investigated a bidirectional bending sensor based on an in-fiber U-shaped Fabry-Perot cavity. Both results of the theoretical analysis and experimental study verify the bending direction dependence and monotonous sensing characteristic at a single direction. The theoretical analysis for the proposed UFPI presents that the sensitivity of the bending sensor is related to the distance between the two cores center of microfiber and SMF end faces, which indicates a new sight into improve the performance of bend sensors based on UFPI. Moreover, the cavity is constructed by just eccentrically splicing a section of microfiber into two SMF end faces and thus, is easy to fabricate and costless. The sensing unit is at the order of 100 μm in length, which indicates a competitive compact size. The low temperature sensitivity will deduce the effect of the crossing-sensitivity and thus improve the bending measurement precision in practical application.

References

[1] S. S. Yin and P. Ruffin, *Fiber Optic Sensors*. Hoboken, NJ, USA: Wiley, 2002.
[2] F. Wang, Z. Shao, J. Xie, Z. Hu, H. Luo, and Y. Hu, "Extrinsic fabry–pérot underwater acoustic sensor based on micromachined center-embossed diaphragm," *J. Lightw. Technol.*, vol. 32, no. 23, pp. 4026–4034, Dec. 2014.

[3] X. Zhang, W. Peng, and Y. Zhang, "Fiber Fabry–Perot interferometer with controllable temperature sensitivity," *Opt. Lett.*, vol. 40, pp. 5658–5661, 2015.
[4] S. Gao *et al.*, "Microfiber-enabled in-line fabry–pérot interferometer for high-sensitive force and refractive index sensing," *J. Lightw. Technol.*, vol. 32, no. 9, pp. 1682–1688, May 2014.
[5] Z. Yang *et al.*, "Extrinsic Fabry–Perot interferometric optical fiber hydrogen detection system," *Appl. Opt.*, vol. 49, pp. 2736–2740, 2010.
[6] X. Liu, I. I. Iordachita, X. He, R. H. Taylor, and J. U. Kang, "Miniature fiber-optic force sensor based on low-coherence Fabry-Pérot interferometry for vitreoretinal microsurgery," *Biomed. Opt. Exp.*, vol. 3, pp. 1062–1076, 2012.
[7] Y. Zhang, H. Shibru, K. L. Cooper, and A. Wang, "Miniature fiber-optic multicavity Fabry–Perot interferometric biosensor," *Opt. Lett.*, vol. 30, pp. 1021–1023, 2005.
[8] M. S. Ferreira *et al.*, "Fabry-Perot cavity based on silica tube for strain sensing at high temperatures," *Opt. Exp.*, vol. 23, pp. 16063–16070, 2015.
[9] C. Liao *et al.*, "High-sensitivity strain sensor based on in-fiber rectangular air bubble," *Sci. Rep.*, vol. 5, 2015.
[10] K. A. Murphy, M. F. Gunther, A. M. Vengsarkar, and R. O. Claus, "Quadrature phase-shifted, extrinsic Fabry–Perot optical fiber sensors," *Opt. Lett.*, vol. 16, no. 4, pp. 273–275, 1991.
[11] J. S. Sirkis, D. D. Brennan, M. A. Putman, T. A. Berkoff, A. D. Kersey, and E. J. Friebele, "In-line fiber etalon for strain measurement," *Opt. Lett.*, vol. 18, no. 22, pp. 1973–1975, 1993.
[12] Y. Wang, D. N. Wang, C. R. Liao, T. Hu, J. Guo, and H. Wei, "Temperature-insensitive refractive index sensing by use of micro Fabry–Pérot cavity based on simplified hollow-core photonic crystal fiber," *Opt. Lett.*, vol. 38, pp. 269–271, 2013.
[13] F. C. Favero, L. Araujo, G. Bouwmans, V. Finazzi, J. Villatoro, and V. Pruneri, "Spheroidal Fabry-Perot microcavities in optical fibers for high-sensitivity sensing," *Opt. Exp.*, vol. 20, no. 7, pp. 7112–7118, Mar. 2012.
[14] D.-W. Duan, Y.-J. Rao, Y.-S. Hou, and T. Zhu, "Microbubble based fiber-optic Fabry–Perot interferometer formed by fusion splicing single-mode fibers for strain measurement," *Appl. Opt.*, vol. 51, pp. 1033–1036, 2012.
[15] C. R. Liao, T. Y. Hu, and D. N. Wang, "Optical fiber Fabry-Perot interferometer cavity fabricated by femtosecond laser micromachining and fusion splicing for refractive index sensing," *Opt. Exp.*, vol. 20, no. 20,pp. 22813–22818, 2012.
[16] T. Wei, Y. Han, H.-L. Tsai, and H. Xiao, "Miniaturized fiber inline Fabry-Perot interferometer fabricated with a femtosecond laser," *Opt. Lett.*, vol. 33, pp. 536–538, 2008.
[17] Z. Yong, C. Zhan, J. Lee, S. Yin, and P. Ruffin, "Multiple parameter vector bending and high-temperature sensors based on asymmetric multimode fiber Bragg gratings inscribed by an infrared femtosecond laser," *Opt. Lett.*, vol. 31, pp. 1794–1796, 2006.
[18] W. Zhang, X. Lei, W. Chen, H. Xu, and A. Wang, "Modeling of spectral changes in bent fiber bragg gratings," *Opt. Lett.*, vol. 40, pp. 3260–3263, 2015.
[19] G. Mao *et al.*, Fiber Bragg grating sensors in hollow single-and two-core eccentric fibers, *Opt. Exp.*, vol. 25, no. 1, pp. 144–150, 2017.
[20] A. Rauf, J. Zhao, B. Jiang, Y. Jiang, and W. Jiang, "Bend measurement using an etched fiber incorporating a fiber Bragg grating," *Opt. Lett.*, vol. 38, pp. 214–216, 2013.
[21] P. Geng *et al.*, "Two-dimensional bending vector sensing based on spatial cascaded orthogonal long period fiber," *Opt. Exp.*, vol. 20, pp. 28557–28562, 2012.
[22] Q. Zhou *et al.*, "Bending vector sensor based on a sector-shaped long-period grating," *IEEE Photon. Technol. Lett.*, vol. 27, no. 7, pp. 713–716, Apr. 2015.
[23] S. Zhang, W. Zhang, S. Gao, P. Geng, and X. Xue, "Fiber-optic bending vector sensor based on Mach–Zehnder interferometer exploiting lateral-offset and up-taper," *Opt. Lett.*, vol. 37, pp. 4480–4482, 2012.
[24] B. Sun *et al.*, "Asymmetrical in-fiber Mach-Zehnder interferometer for curvature measurement," *Opt. Exp.*, vol. 23, no. 11, pp. 14596–14602, 2015.
[25] S. Gao, W. Zhang, P. Geng, X. Xue, H. Zhang, and Z. Bai, "Highly sensitive in-fiber refractive index sensor based on down-bitaper seeded up-bitaper pair," *IEEE Photon. Technol. Lett.*, vol. 24, no. 20, pp. 1878–1881, Oct. 2012.
[26] Z. Bai *et al.*, "Compact long period fiber grating based on periodic micro-core-offset," *IEEE Photon. Technol. Lett.*, vol. 25, no. 21, pp. 2111–2114, Nov. 2013.
[27] Z. Bai, W. Zhang, S. Gao, H. Zhang, L. Wang, and F. Liu, "Bend-insensitive long period fiber grating-based high temperature sensor," *Opt. Fiber Technol.*, vol. 21, pp. 110–114, 2015.